Electronic Structure, Biological Activity, Spectral Analysis, NBO, NLO, and Thermodynamic Properties of 3-Chloro-4-Hydroxyquinolin-2(1H)-One. DFT Approach

Hussien, Shimaa Abdel Halim*+

Department of Chemistry, Faculty of Education, Ain Shams University, Roxy 11711, Cairo, EGYPT

ABSTRACT: *Chlorination of 3-acetyl-4-methylthioquinolin-2(1H)-one (1) with sulfuryl chloride may lead to 3-(2,2-dichloroacetyl)-4-methylthioquinolin-2(1H)-one (2). Whereas analytical and spectral results for the product of this reaction evoked the proposal of obtaining 3-chloro-4-hydroxyquinolin-2(1H)-one (3), which was found by reduction of 3,3-dichloroquinolin-2,4-dione. Density Functional Theory (DFT) and time-dependent density functional theory (TD-DFT) calculations of the electronic structure at the B3LYP/6-311++G (d,p) level of theory were used to investigate the geometries, linear polarizability ⟨Δα⟩, first order hyperpolarizability ⟨β⟩, natural bonding orbital (NBO), molecular electrostatic potential contours (MEP&ESP), electrophilicity (ω), and UV-Vis spectra, in both ethanol and dioxane solvents for compound 3. The geometrical and energetic characteristics have been thoroughly studied to determine why compound 3 was formed instead of another expected result compound 2. At the same time, the thermo-chemical parameters, NMR, harmonic vibration frequencies, and equilibrium geometries were computed. The calculated acidity constant (pKa) for the protonated and deprotonated forms in ethanol for the present compound 3. Band maxima (λ_{max}) and spectra intensities are reflected as blue and red shifts in the solvent dependence. The excited state was identified and contributed to the electronic configurations. Finally, DFT calculations were used to connect the structure-activity relationship (SAR) with real antibacterial results for compound 3.*

KEYWORDS: UV-Vis spectra; DFT/TD-DFT; NBO/NLO analysis; FT-IR; Thermodynamic properties; Vibration analyses**;** NMR**;** Antimicrobial.

INTRODUCTION

Quinolinones are used to treat genitourinary infections, prostate, and respiratory diseases, sexually transmitted diseases, gastroenteritis, and skin and soft tissue infections [1]. Quinolinones have antitumor [2], anti-HSV [3], anticonvulsant, [4] anti-oxidation and anti-inflammatory activity [5-7], and bactericidal, fungicidal, and molluscicide activity [8]. The importance of this heterocyclic category drew our attention to the chlorination of 3-acetyl-4-methylthioquinolin-2(1H)-one (1) with sulfuryl chloride, which results in 3-(2,2-dichloroacetyl)-4-methylthioquinolin-2(1H)-one (2). While the analytical and spectral results for the reaction's product suggested that 3-chloro-4-hydroxyquinolin-2(1H)-one may be obtained (3). Which was found by reducing

**To whom correspondence should be addressed.*

+ E-mail: Shimaaquantum@ymail.com

1021-9986/2023/9/3019-3038 20/$/7.00

3,3-dichloroquinolin-2,4-dione, (*Ziegler et al.*, 1962), [9]. Finding new drug candidates and establishing the electrical structure of molecular systems need computational investigation based on density functional theory. The Density Functional Theory (DFT) method has been popular for confirming experimental values of molecular geometry, vibrational frequencies, atomic charges, dipole moment, thermodynamic characteristics, and so on [10–19]. Thus, the present research work aims to investigate of the electronic structure and spectra of compound 3 experimentally and theoretically also; predicted the biological activity for compound 3. In addition to providing a systematic investigation of the experimental UV-Vis spectra of 3 utilizing TD-DFT computations at the Coulomb-attenuating method (CAM- B3LYP/6-311++G (d, p)) and Corrected Linear Response Polarizable Continuum Model (CLR) PCM were used to obtain the theoretical electronic absorption spectra in the gas phase, ethanol, and dioxane solvents, respectively, indicating a good agreement with the observed spectra. The Natural Bond Orbital (NBO) analysis study characterizes the charge transfer of the electron density over 3. Additionally, structural, FT-IR, NMR, and vibrational studies, thermo-chemical parameters, Molecular Electrostatic Potential (MEP), and electronic properties including the HOMO-LUMO energy gap, chemical hardness, and chemical potential were carried out. The electronic dipole moment (μ), first-order hyperpolarizability (β), hyper-Rayleigh scattering (β_{HRS}), and Depolarization Ratio (DR) are Non-Linear Optical (NLO) parameters that were calculated on the same theoretical level. At the B3LYP/6-311++G (d, P) theoretical level, the DFT method was employed to complete all computations in this study. The calculated acidity constant (pKa) for the protonated and deprotonated forms in ethanol for the present compound 3. The antibacterial application was also used to investigate the Structure-Activity Relationship (SAR) for the present compound 3 [20].

EXPERIMENTAL SECTION

Chemicals Used

The target compound 3-chloro-4-hydroxyquinolin-2(1H)-one (3). was synthesized as follows:

To a stirred solution of the 3-acetyl-4-methylthioquinolin-2(1H)-one (1) (10 m mol, 2.33 g) at room temperature, sulfuryl chloride (5 mL, 50 m mol) was added for 30 minutes in dioxane (50 mL). Afterward, the reaction mixture was poured into crushed ice. The so-obtained pale yellow precipitate was collected, filtered, dried, and crystallized from absolute ethanol to give compound 3-chloro-4-hydroxyquinolin-2(1H)-one (3), yield: 1.3 g (66%), m. p. 275—277◦C (decomp.) [9]. I remove a single crystal from the sample (compound 3), which is depicted in Fig. 1 and describes the system as KBr discs (all IR) by the ratio (1:20). IR (KBr, cm^{-1}), ν: 3249 (H-bonded O–H), 3196 (N-H), 3063 (C-H_{arom}), 2957 (C-H_{aliph}), 1751 (C-$O_{carboxylic}$), 1690 (C-$O_{\alpha\text{-keto}}$), and 1632 (C-$O_{quinolone}$).

Apparatus

Correcting melting points is not done and were determined in open capillary tubes on a digital Stuart-SMP3 apparatus. IR spectra were recorded on a Perkin-Elmer FT-IR 1650 spectrophotometer, using samples in KBr disk. Parkin Elmer lambda 4B spectrophotometer was used to measure the electronic absorption spectra using 1.0 cm fused quartz cells. The machine records linearly the percent of transmittance over the range 200-900 nm.

Solvents

A Polar (ethanol) and non-polar (dioxane) solvents were obtained from Merck, AR-grade, and used without further purification. The concentration of the solute is 2.036×10^{-4} mol/L in polar solvent and 1.131×10^{-4} mol/L in non-polar solvent.

Antimicrobial study

Antibacterial and antifungal capabilities of produced compound 3 were investigated against several bacteria, including Gram-positive *S.* aureus and *B. subtilis*, and Gram-negative *S. Typhimurium* and *E. Coli*, as well as *yeast*, *C. albicans*. *A. fumigatus* is a species of *A. fumigatus*.

Computational details

The Gaussian 09 program package [21] was used to do the computations in this work, and the results were evaluated using the Gauss-view 05 molecular visualization program [22]. DFT [23-26] using a hybrid functional B3LYP [27], combines the Lee–Yang–Parr (LYP) correlation functional [28] with Beck's three parameters

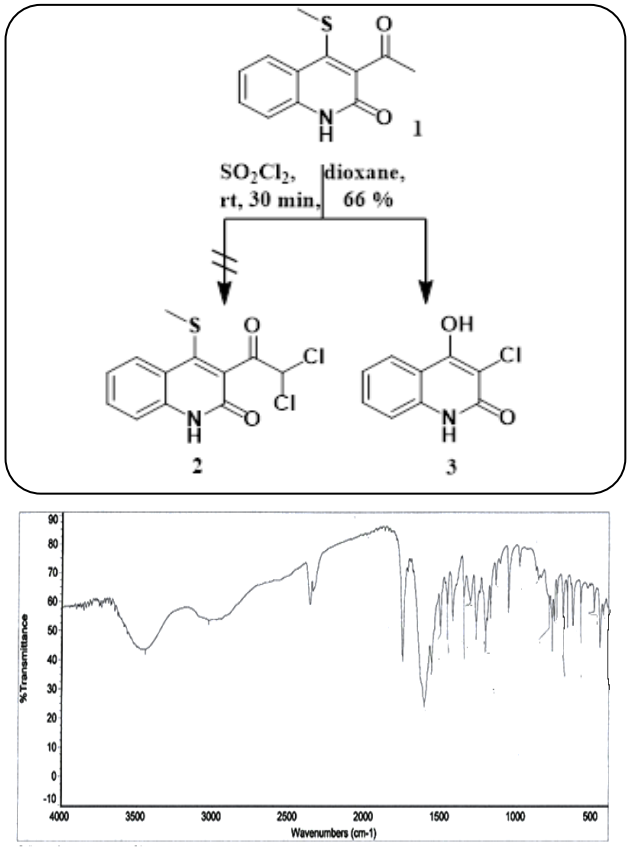

Scheme 1: Chlorination reaction for compound 1 to give compound 3, not 2

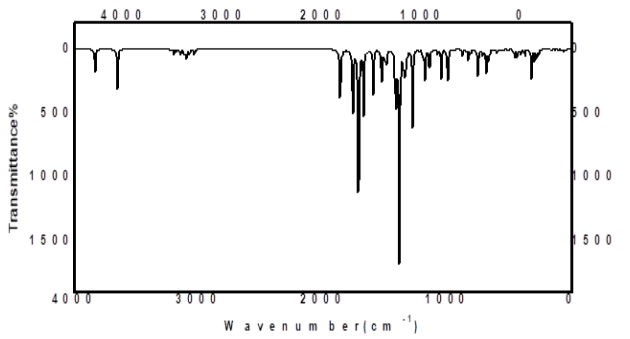

Fig. 1: Experimental and Calculated IR spectra for (3) at B3LYP/6-311++G (d,p)

(local, non-local, Hartree–Fock) hybrid exchange functional (B3), and the Coulomb Attenuating Method (CAM-B3LYP) [28] were used to obtain optimized geometrical parameters, vibrational frequencies, determine UV–Vis spectra, electronic transitions, and electronic characteristics such as HOMO–LUMO energies for the title compound 3. B3LYP For a better representation of polar bonding in molecules, the basis set 6-311++G(d,p) with 'd' polarization functions on heavy atoms and 'p' polarization functions on hydrogen atoms were utilized [29]. Using the same level of theory, NMR chemical shifts were estimated using the Gauge Including the Atomic Orbital (GIAO) approach [30]. On the NBO basis, the donor–acceptor interactions were evaluated using the second order Fock matrix [31]. The antibacterial application was also used to investigate the Structure-Activity Relationship (SAR) for the present compound 3. Also, the following equations were calculated for the total static dipole moment (μ), $\langle\Delta\alpha\rangle$, and $\langle\beta\rangle$, values.

$$\mu = (\mu^2_x + \mu^2_y + \mu^2_z)^{1/2},$$

$$\langle\alpha\rangle = 1/3\,(\alpha_{xx} + \alpha_{yy} + \alpha_{zz}),$$

$$\Delta\alpha = ((\alpha_{xx} - \alpha_{yy})^2 + (\alpha_{yy} - \alpha_{zz})^2 + (\alpha_{zz} - \alpha_{xx})^2/2)^{1/2},$$

$$\langle\beta\rangle = (\beta^2_x + \beta^2_y + \beta^2_z)^{1/2}, \quad (1)$$

Where:

$$\beta_x = \beta_{xxx} + \beta_{xyy} + \beta_{xzz},$$

$$\beta_y = \beta_{yyy} + \beta_{xxy} + \beta_{yzz},$$

$$\beta_z = \beta_{zzz} + \beta_{xxz} + \beta_{yyz}. \quad (2)$$

Using the predicted energies of HOMO and LUMO, global reactivity descriptors were calculated as follows: $\chi = (I + A)/2$ (electronegativity), $\eta = (I - A)/2$ (chemical hardness), $S = 1/2\eta$ (global softness), $\omega = \mu^2/2\eta$ (electrophilicity) where I and A were ionization potential and electron affinity, and $I = -E_{HOMO}$ and $A = -E_{LUMO}$, respectively. For the conversion factors of α, β, and HOMO and LUMO energies in atomic and cgs units: 1 atomic unit (a.u.) = 0.1482×10^{-24} electrostatic unit (esu) for polarizability $\langle\alpha\rangle$; 1 a.u. = 8.6393×10^{-33} esu for first hyperpolarizability $\langle\beta\rangle$; 1 a.u. = 27.2116 eV for HOMO and LUMO energies [32-35].

RESULTS AND DISCUSSION

Chemistry

Chlorination of 3-acetyl-4-methylthioquinolin-2(1H)-one (1) with sulfuryl chloride may lead to 3-(2,2-dichloroacetyl)-4-methylthioquinolin-2(1H)-one (2). Whereas analytical and spectral results for the product of this reaction evoked the proposal of obtaining 3-chloro-4-hydroxyquinolin-2(1H)-one (3), which was found by reduction of 3,3-dichloroquinolin-2,4-dione. (Scheme 1).

Table 1: Experimental and calculated wave number, IR intensities, and assignments for 3-chloro-4-hydroxyquinolin-2(1H)-one (3), at the B3LYP/6-311++G (d,p).

No.	$\upsilon_{exp.}$(cm^{-1}) [9, 37, 38]	$\upsilon_{the.}$ (cm^{-1}) un-scaled	$\upsilon_{the.}$ (cm^{-1}) scaled	Intensity	Assignment
1	2800-3447 3249	3445	3312	95.37	H-bonded-O-H Stretching
2	3196	3384	3253	97.84	NH Stretching
3	3000-3100 3063	3190	3067	12.83	C-H aromatic Asym Stretching
4	2850-3000 2957	3076	2957	16.01	C-H aliphatic Sym Stretching
5	1751-1755 1751	1763	1695	223.48	C=O carboxylic group Sym Stretching
6	1690-1695 1690	1716	1650	612.76	C=O ketonic group Asym Stretching
7	1400-1600 1632	1673	1608	158.25	C=O quinoline Sym Stretching

The experimental and theoretical IR spectra of the studied compound 3 in Fig. 1 and Table 1 showed characteristic two strong stretching absorption bands at ν 1751–1755 cm^{-1} due to carboxylic C=O group and ν 1690–1695 cm^{-1} due to ketonic C=O group.

Analysis of vibrations

Compound 3 has 19 atoms and 51 normal modes of vibration, and it has a C1 point group symmetry. The computed and recorded FT-IR spectra are shown in Fig. 1. The FT-IR experimental frequencies, unscaled and scaled vibrational frequencies, of compound 3 were computed using the B3LYP technique with the 6–311++G (d,p) basis set, as shown in Table 1. The difference in theoretical and experimental frequencies is attributable to the overestimation of force constants in quantum calculations. To bring the experimental and theoretical differences closer together, the theoretical values are scaled with a 0.9613 scaling factor [36]. The computed vibration is ascribed to N–H symmetric stretching vibration at 3384 cm^{-1} (unscaled value) and 3253 cm^{-1} (scaled value), which has shown a similar correlation with experimental data at 3196 cm^{-1}. The aromatic C–H stretching vibrations [37] are in general observed in the region 3000–3100 cm^{-1}. The computed vibration is assigned to C–H aromatic stretching vibrations at 3190 cm^{-1} (un-scaled value) and 3067 (scaled value) for compound 3 which is comparable with experimental results at 3063 cm^{-1}. The computed vibration is assigned to symmetric C–H aliphatic stretching vibration at 3076 (un-scaled value) and at 2957 (scaled value) for compound 3 has shown a comparable agreement with experimental results at 2957 cm^{-1}. The computed vibration is assigned to asymmetric H-bonded-O-H stretching vibration at 3445 cm^{-1} (un-scaled value) and at 3312 (scaled value) for compound 3 which has shown a comparable agreement with experimental results at 2800-3447 cm^{-1} (3249 cm^{-1}). Generally, the C=O vibrations [38] are observed in the region 1790-1810 cm^{-1}. Vibrations are assigned to C=O carboxylic group Sym stretching vibration at 1763 cm^{-1} (un-scaled value) and at 1695 (scaled value) for compound 3 which is comparable with experimental results at 1751 cm^{-1}. The Computed vibration is assigned to C=O ketonic group Asym stretching vibrations at 1716 cm^{-1} (un-scaled value) and at 1650 (scaled value) for compound 3 which is comparable with experimental results at 1690 cm^{-1}. The computed vibration is assigned to asymmetric C=O quinoline Sym stretching vibration at 1673 cm^{-1} (un-scaled value) and at 1608 (scaled value) for compound 3 has shown a comparable agreement with experimental results at 1632 cm^{-1}.

Theoretical study

The goal of this work is to investigate the ground state electronic properties of compound 3, using DFT calculations at the B3LYP level of theory and the basis set 6-311++G (d,p) in addition to proving the proposed mechanism discussed in Scheme 1. The theoretical calculations show why the prepared compound 3 is unstable experimentally as compared with the unprepared compound 2. The total energy computed theoretically of compound 2 is (E_{total} = -1986.748 a.u.) while compound 3

Table 2: The Optimized calculations of 2 and 3 compounds and a comparative analysis of 3 with the similar types of compounds at the B3LYP/6-311++G(d,p)

Parameters	2	3	Ref. [10]	Ref. [11]	Ref. [12]	Ref. [15]
Total Energy, (E_T) (a.u.)	-1986.7481	-1012.1646				
Energy of highest occupied molecular orbital (E_{HOMO}) (eV)	-6.8250	-6.4902	-6.5560	-6.2843	-6.6645	-6.391
Energy of lowest unoccupied molecular orbital (E_{LUMO}) (eV)	-2.7692	-2.0705	-2.5359	-2.5013	-2.7564	-2.581
Energy Gap, (E_g) (eV)	4.0558	4.4197	4.02016	3.7830	3.9080	3.810
Dipole moment, (μ)	6.9299	6.9999	7.8870	5.3982	1.0896	4.28
I (eV)	6.8250	6.4902	6.55602	6.2843	6.9208	6.391
A(eV)	2.7692	2.0705	2.53586	2.5013	3.7830	2.581
X(eV)	4.7971	4.2803	4.54594	4.3928	5.3519	4.486
V(eV^{-1})	-4.7971	-4.2803	-4.54594	-4.3928	-5.3519	-4.486
η(eV)	2.0279	2.2098	2.01008	1.8915	1.5689	1.905
S(eV^{-1})	0.2466	0.2262	0.24875	0.2643	0.3187	0.263
ω (eV)	5.6739	4.1453	5.14048	5.1009	7.3293	5.2819

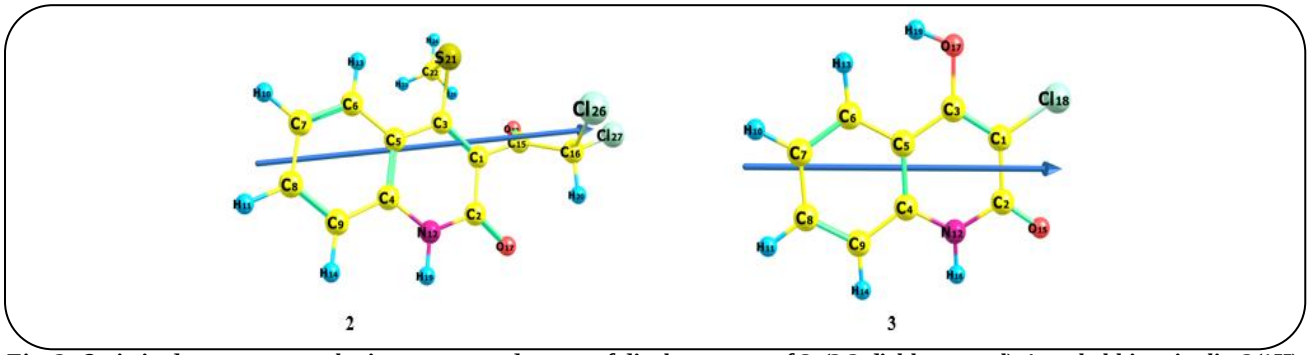

Fig. 2: Optimized geometry, numbering system, and vector of dipole moment of 3-(2,2-dichloroacetyl)-4-methylthioquinolin-2(1H)-one (2) and 3-chloro-4-hydroxyquinolin-2(1H)-one (3), using B3LYP/6-311++G(d,p)

is (E_{total} = -1012.164 a.u.) and E_{total} for C_3H_3SCl group is (E_{total} = - 974.511 a.u.). As shown in the equation depicted below, the molecular formula of unexpected compound 2 is equal to the molecular formula of expected compound 3 plus C_3H_3SCl group. i.e.

Compound 2 ($C_{12}H_9NCl_2SO_2$) = Compound 3 ($C_9H_6NClO_2$) + C_3H_3SCl group

E_{total} = E_{total} + E_{total}

-1986.7 = - 1012.164 - 974.511

-1986.748 a.u. = -1986.675 a.u.

it's clear from the above equation that the total energy of compound 3 plus C_3H_3SCl group has more energy than compound 2 alone by deference in value 0.073 a.u., 1.9856 eV (≈ 46 kJ/mol). Therefore, the result will be that the energy of compound 2 is lower than compound 3. Therefore, the reaction of compound 2 formation is more dominant, but experimentally not formation the compound 2, and separated the reaction media for compound 3 only (c.f. Scheme 1). So that I used theoretical calculation to explain this the reaction. The energetic and ground state properties of compound 3 are listed in Table 2.

Table 2 shows that the computed energy gap (Eg) for compound 2 is less than compound 3 by 8.4 kJ/mol, indicating that compound 2 has higher reactivity than compound 3. Furthermore, compound 3 has a greater computed dipole moment (μ) than compound 2, and the vector of dipole moment for compound 3 is in the same direction as compound 2 (Fig. 2), indicating that compound 3 has a higher polarity than compound 2. Table S1 showed that the electron density of compound 2 was concentrated at positions C1 and C3, indicating the elevated nucleophilicity of C1 and C3 in comparison to other carbon atoms and supporting the proposed mechanism illustrated in Scheme 1. In addition, in compound 3 all the charge

Table S1: Mullikan (MPA) and natural (NAC) charges for studied compounds 2 and 3 at the B3LYP/6-311++G(d,p)

Atoms.	Mullikan charges		Natural charges	
	2	3	2	3
N12	-0.126	-0.136	-0.555	-0.572
Cl18	0.223	0.330	0.024	0.062
Cl26	-0.049	-------	-0.008	-------
S21	-0.044	-------	0.223	-------
O15	-0.318	-0.296	-0.496	-0.606
O17	-0.146	-0.144	-0.638	-0.641
C1	0.420	0.039	-0.211	-0.182
C2	-0.090	-0.282	0.643	0.618
C3	1.468	-0.044	-0.059	0.341
C4	-0.000	-1.271	0.209	0.207
C5	0.512	1.908	-0.136	-0.147
C6	-0.649	-0.200	-0.139	-0.161
C7	-0.459	-0.065	-0.225	-0.226
C8	-0.344	-0.309	-0.159	-0.171
C9	-0.629	-0.718	-0.234	-0.226
H16	0.343	0.331	0.407	0.405
H19	0.335	0.293	0.261	0.213
H13	0.147	0.069	0.204	0.189
H14	0.166	0.145	0.211	0.189
H11	0.183	0.175	0.228	0.211
C15	-0.995	-------	0.565	-------
C16	-0.310	-------	-0.307	-------
C22	-0.785	-------	-0.682	-------

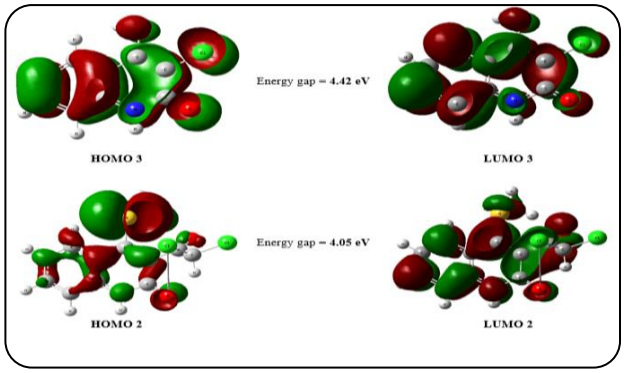

Fig. 3: HOMO, LUMO, and energy gap of 3-(2,2-dichloroacetyl)-4-methylthioquinolin-2(1H)-one (2) and 3-chloro-4-hydroxyquinolin-2(1H)-one (3), using B3LYP/6-311++G(d,p)

density of the HOMO localized on quinoline moiety compared with other moieties (Fig. 3) in contrast to compound 2. Furthermore, the high stability of the synthesized compound 3 as determined by the computed total energy agrees well with results obtained from mass spectrometry of this molecule [9], which indicated the molecular ion peak as a base peak, confirming the stability of the generated compound 3. A comparison of the obtained results with those published for similar structures is listed in Table 2. It is clear from the table that the values of the obtained parameters for 3 are close to the values obtained for similar structures, considering the computational error percent, which confirms the accuracy of the obtained results [10-12,15].

Study the geometrical structure

Fig. 2 describes the theoretically potential best geometrical configurations of compound 3 with atom numbering. Table 3 illustrates the internal coordinates, which characterize the position of atoms in terms of distances, angles, and dihedral angles for an origin atom. The C–C single bond and the C=C double bond are shared

Table 3: Equilibrium bond lengths, (Å), bond angles, (°), and Dihedral angles, (°) for studied compounds 2 and 3 at the B3LYP/6-311++G(d,p)

Parameters	2	3	Exp. [39-41]
Bond lengths (Å)	1.777		
C_1-Cl_{18}	1.811	1.731	1.790
C_{16}-Cl_{26}	1.826	------	1.790
C3-S21	1.202	------	1.821
C_2- O_{15}	1.227	1.218	1.241
C_3-O_{17}	1.379	1.351	1.321
C4-N12	1.370	1.375	1.358
C-C	1.472	1.463	1.487
C=C	1.366	1.365	1.340
O-H	------	0.962	1.025
Bond angles (°)	108.83		
$<C_1C_2Cl_{18}$	112.12	116.72	117.61
$<C_1C_3Cl_{18}$	111.74	120.92	118.44
$<Cl_{26}C_{16}Cl_{27}$	100.37	--------	117.61
$<C_3S_{21}C_{22}$	120.28	--------	105.84
$<C_3S_{21}C_1$	121.96	--------	118.57
$<C_1C_3O_{17}$	122.02	118.61	119.94
$<O_{17}C_3C_5$	124.43	120.65	121.21
$<C_1C_2O_{15}$	120.76	125.84	125.52
$<O_{15}C_2N_{12}$	114.80	120.46	119.67
$< C_1C_2N_{12}$	125.99	113.70	112.87
$<C_2N_{12}C_4$	120.46	126.42	126.53
$<C_9N_{12}C_4$	118.80	121.00	120.25
$< C_5C_4N_{12}$		118.89	117.65
Dihedral angles (°)	125.23		
$<Cl_{18}C_1C_3O_{17}$	1.095	-0.269	
$< Cl_{18}C_1C_2O_{15}$	-120.37	0.340	
$< Cl_{26}C_{16}H_{20}Cl_{27}$	91.081	-------	
$< C_{22}S_{21}C_3C_1$	-177.63	-------	
$< S_{21}C_3C_5C_4$	-177.47	-------	
$<O_{17}C_3C_1C_2$	118.82	-179.90	
$<O_{15}C_3C_1C_2$	1.117	179.99	
$<N_{12}C_4C_5C_3$	-1.707	0.744	
$<N_{12}C_4C_2C_1$	1.777	-0.859	

by compounds 2 and 3. For C–C, the bond length predicted using the computing technique is 1.472, 1.463 Å, and C=C, is 1.366, 1.365 Å, which are almost identical to the experimental result [39-41]. The bond lengths of C2–O15, and C3–O17 in two compounds 2 and 3 in the theoretical (gaseous phase) are 1.227, 1.218 Å, and 1.379, 1.351 Å, respectively, which are shorter than the experimental values due to phase transitions (solid phase). With sp^2 hybridization, the bond angles should be 120°, however, they vary from 117° to 126°, which could be related to substitution effects. Due to electronic conjugation among the bonds and the presence of an oxygen atom, there

are slight deviations in bond angles from the predicted value of 120°.

Frontier molecular orbital analysis

Red and green colors characterize the positive and negative phases of the HOMO and LUMO, the green instead of the highest attraction and red indicating the strongest repulsion, respectively (Fig. 3). As shown in Fig. 3, the HOMO is placed over the C=C bond in the quinoline ring, whereas the LUMO is placed over the oxygen and nitrogen atoms of both molecules 2 and 3. For compound 3, the HOMO molecule orbital has an energy of -6.49 eV, whereas the LUMO molecular orbital has an energy of -2.07 eV. The HOMO and LUMO molecular orbitals have a 4.42 eV energy difference.

Table 2 lists the electronic parameters as well as the global reactivity descriptors. The HOMO-LUMO orbitals are the Frontier Molecular Orbitals (FMO). The difference in energy between HOMO and LUMO is an important measure of kinetic stability. According to the wave function, electron absorption is predominantly represented by one electron promotion and corresponds to the transition from HOMO to LUMO. The Koopmans' hypothesis was used to investigate the global reactivity descriptor parameters and calculate various parameters such as ionization potential (*I*), electron affinity (*A*), band gap (Eg), electronegativity (χ), absolute hardness (η), global softness (*S*), global electrophilicity (ω), and chemical potential (*V*). According to the research, the molecule in [11] has the smallest band energy gap, which makes charge transfer inside the molecule easier. When it comes to HOMO and LUMO reactivity, the molecule in [11] has the most reactive HOMO, whereas 3 and [10, 12] have the most reactive LUMO. In the current molecule 3, the maximum charge transfer occurs. The molecule in [10] has a higher absolute hardness value (η = 2.01) than the molecule in [12], but a lower global softness value (*S* = 0.25). The values of several parameters change significantly between 3 and Ref. [10-12, 15] molecules.

Molecular Electrostatic Potential (MEP)

The quinoline ring had the strongest affinity for a proton, with the maximum negative region (nucleophilic) indicated in red and the maximum positive region (electrophilic) shown in blue around the quinoline ring, suggesting the strongest attraction for electrons in Fig. S1. Furthermore, the atom N12 has a neutral potential, whereas the atoms O15, O17, and Cl18 have a very repulsive potential.

The 3D plots of the Highest Occupied Molecular Orbital (HOMO) and the Lowest Unoccupied Molecular Orbital (LUMO), Electrostatic Potential (ESP), Electron Density (ED), and the Molecular Electrostatic Potential

(MEP) map for the title molecule at the B3LYP method with 6-311++G (d,p) level are shown in Fig. S1. The ED plot for the title molecule shows a uniform distribution. While the negative ESP is localized more over the oxygen atoms, the positive ESP is localized on the rest of the title molecule.

MEP has been used primarily for predicting sites and relative reactivity towards electrophilic and nucleophilic attack and in studies of biological recognition and hydrogen bonding interactions [42-44]. The calculated 3D MEP of the title compound was calculated from the optimized molecular structure by using the B3LYP/6-311++G (d,p) level also shown in Fig. S1. The color scheme for the MEP surface is as follows: red for electron-rich, partially negative charge; blue for electron deficient, partially positive charge; light blue for slightly electron deficient region; yellow for slightly electron-rich region; green for neutral (zero potential); respectively [45]. According to our results, the negative region (red) is mainly over the O atomic sites, which were caused by the contribution of lone-pair electrons of the oxygen atoms while the positive (blue) potential sites are around the hydrogen and carbon atoms. A portion of a molecule that has a negative electrostatic potential will be susceptible to electrophilic attack—the more negative is the better. It is not as straightforward to use electrostatic potentials to predict the nucleophilic attack. Hence, the negative region (red) and positive region (blue) indicate electrophilic and nucleophilic attack symptoms. Also, a negative electrostatic potential region is observed around the O atom.

Global reactivity descriptors

Table 2 shows the calculated values of the global reactivity descriptors for the title chemical. DFT-based descriptors such as global hardness (η), global softness (S), electronegativity (χ), and electrophilicity index (ω) are used to define the reactivity and selective site of various biomolecules. A molecule's electrophilicity is used to predict its biological activity, toxicity, and other characteristics.

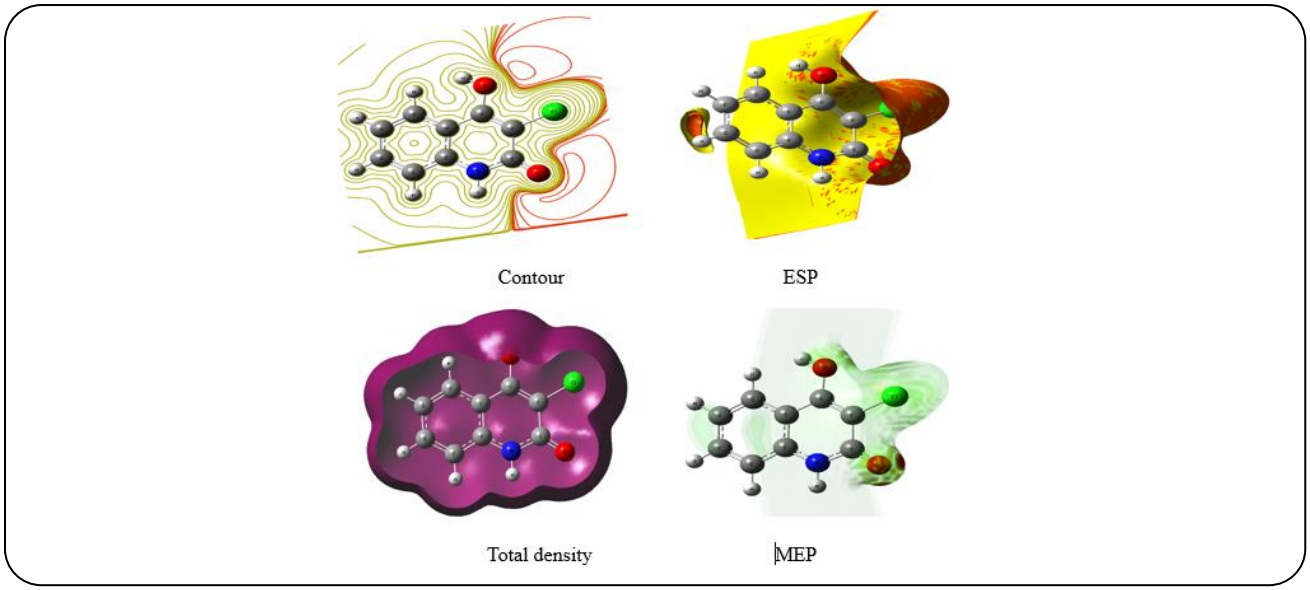

Fig.S1. Molecular surfaces of 3-chloro-4-hydroxyquinolin-2(1H)-one (3), using B3LYP/6-311++G (d,p)

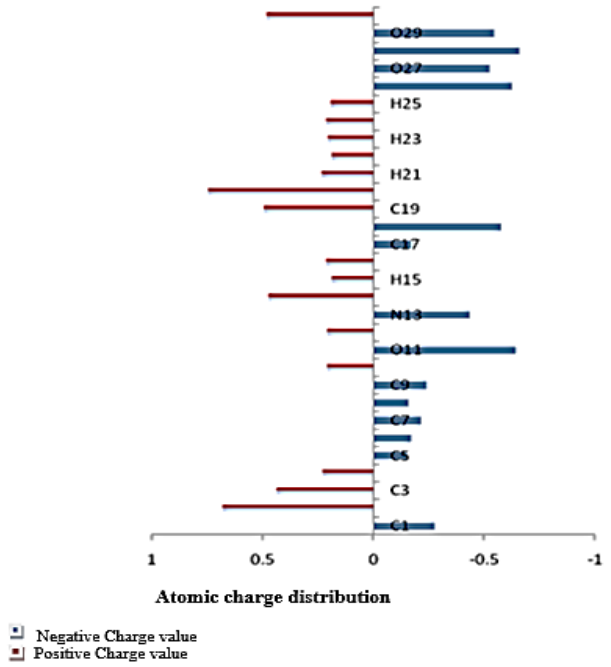

Fig.S2: Atomic charge distribution for 3-chloro-4-hydroxyquinolin-2(1H)-one (3), using B3LYP/6-311++G (d,p)

The biological activities of the molecule are linked to the LUMO energy orbital, electrophilicity, and van der Waals surface area. The electrophilicity index (ω) of a molecular system is a measure of electrophilic power toward a nucleophile. If the electrophilicity index increases, the reactivity of the electrophile will be increased, while if it is decreased, the reactivity of the nucleophile will be increased. In this study, the computed electrophilicity index (ω) was 4.14 eV, which is high, indicating the strong electrophilic reactivity of the current compound. According to MEP, the stability of a molecule increases with hardness at constant external potential, while the reactivity decreases with increasing instability. The calculated HOMO-LUMO energy gap is (4.4197 eV), hardness is 2.2098 eV (gas phase), and the global softness is 0.2262 eV, indicating that the studied compound **3** has high reactivity and more softness.

Atomic charge analysis using natural and mullikan methods

The population matrix, which is based on the molecule's wave function, is generated using in Linear Combination Atomic Orbitals (LCAO), density matrix (P), and overlap matrix (S). Mullikan Polar Atomic Charge analysis (MPA) explains the atomic charges, dipole moment, electrical structure, and biological activity of the molecule. As the charge of an atom increases, the biological activity increases also [46]. Mulliken Polar Atomic Charge Analysis (MPA) and Natural Atomic Charge (NAC) analysis estimate and compare charges over compound 3 and compound 2. (Table S1). According to MPA, the electronic charge on the C1 of both compounds 3 and 2 was reorganized. In compounds 2 and 3, the charges on C1 and C5 are positive, whereas the others are negative. In the two molecules, C5 is very positive, C9 and C22 are highly negative, C1 is very low positive, and C2 is very low negative. Charges on C2 and C4 are positive corresponding to Natural Atomic Charge (NAC),

Table 4: Second Order Perturbation Interaction Energy Values Computed in the NBO Basis for the studied compound 3, calculated at B3LYP/6-311++G (d, p)

Donor	Acceptor	$E^{(2)a}$(kcal/mol)	NBO	Population
πC1- C3	π*C2-O15	21.53	πC1- C3	1.80785
πC4-C5	π*C6-C7	21.87	πC4-C5	1.59248
LP (1) N12	π*C2-O15	50.73	LP (1) N12	1.63777
LP (1) N12	π*C4-C5	49.39	LP (2) O15	1.85734
LP (2) O15	σ*C1-C2	19.05	LP (2) O17	1.85219
LP (2) O15	σ*C2-N12	27.67	LP (2) Cl18	1.96229
LP (2) O17	RY*H19	39.84	π*C2-O15	0.34797
LP (2) O17	π*C1-C3	33.77	π*C6-C7	0.31632
LP (2) O17	σ*O17-H19	19.30	σ*C1-C2	0.07323
LP (2) Cl18	π*C1-C3	14.45	π*C1-C3	0.30949
π*C1- C3	π*C2-O15	190.29	σ*C2-N12	0.08447
π*C4-C5	π*C8-C9	279.69	RY*H19	0.00035
			σ*O17-H19	0.01038
			π*C8-C9	0.30932

[a] $E^{(2)}$ means energy of hyperconjugative interactions (stabilization energy).
$LP_{(n)}$ is a valence lone pair orbital (n) on the atom.

whereas charges on other atoms are negative. Positive charges are associated with carbon in the quinoline ring in all H, whereas negative charges are when attached to oxygen and nitrogen. (In Fig. S2, it is a Mullikan charge).

Natural Bonding Orbital (NBO) analysis

Inter- and intramolecular interactions, as well as charge transfer from an electron donor to an acceptor, were investigated using NBO analysis [47]. For each donor-acceptor (*i*) and (*j*), interaction, the stabilization energy $E^{(2)}$ with the delocalization $i \rightarrow j$ was determined using the second-order Fock matrix, as indicated in the following equation.

$$E^{(2)} = \Delta E_{ij} = q_i (F(ij)2 / \varepsilon j - \varepsilon i), \quad (1)$$

Where q_i is the occupancy donor orbital, ε_i, and ε_j are diagonal elements, and (*i*j) is the NBO Fock matrix with off-diagonal members. The high stabilizing energy for these transitions shows just how possible they are to occur. The larger the interacting stabilization energy $E^{(2)}$ value, the more intensive is the interaction between electron donors and the greater the extent of conjugation of the whole system. Delocalization of electron density between occupied Lewis's type (bond or lone pair) NBO orbitals and formally unoccupied (antibonding or Rydberg) non-Lewis NBO orbitals correspond to a stabling donor-acceptor interaction. The molecular interaction is formed by the orbital overlap between σ (C-C) and σ* (C-C) bond orbital which results in the intramolecular charge (ICT) causing stabilization of the system. These interactions are observed as an increase in Electron Density (ED) in the C-C antibonding orbital that weakens the respective bonds. The electron density of the conjugated double as well as the single bond of the conjugated ring (≈ 1.9e) demonstrates strong delocalization inside the molecule. The highest four most likely transitions in this molecule can be placed in descending order based on the stabilization energy as follows: LP (1) N12 → π*C2-O15, LP (2) O17 → RY*H19, πC1-C3 → π*C2-O15, and πC4-C5 → π*C8-C9. The large stabilization effects are accounted for by the strong lone pair-anti-bonding orbital interactions between the two ends of the produced H-bond. Furthermore, the forbidden character of the transitions was not observed in their UV-Visible spectra. Only the selection rules showed the peaks in both theoretical and experimental spectra, allowing only a few transitions to be discovered by anticipated HOMO-LUMO analysis using the oscillator strengths of the bands. Table 4 shows the types of bonds, acceptors, donors, occupancy levels, and stabilization energy (E^2), all these related data explain the stability of 3.

Table 5: Natural Charge, Natural Population and Natural electronic Configuration of active sites in studied compound 3 using B3LYP/6-311++G (d,p)

Atom No.	Natural Charge	Natural Population				Natural electronic Configuration
		Core	Valence	Rydberg	total	
N12	-0.57183	1.999	5.558	0.0142	7.572	[core]2S (1.25)2p (4.31)4p (0.01)
O15	-0.60650	1.999	6.594	0.0131	8.606	[core]2S (1.70)2p (4.90)3d (0.01)
O17	-0.64097	1.999	6.628	0.0131	8.641	[core]2S (1.65)2p (4.98)3p (0.01)
Cl18	0.06210	9.999	6.915	0.0228	16.94	[core]3S (1.83)3p (5.08)3d (0.01)4p (0.01)

For the numbering system, see Fig. 2

Table S2: Natural population of the total electrons in studied compound 3 using B3LYP/6-311++G (d,p)

Parameters	3
Core	33.98892 (99.967% of 34)
Valence Lewis	63.57317 (96.323% of 66)
Total Lewis	97.56208 (97.562% of 100)
Valence non-Lewis	2.24560 (2.246% of 100)
Rydberg non-Lewis	0.19231 (0.192% of 100)
Total non-Lewis	2.43792 (2.438% of 100)

Natural population analysis and natural charges

At the B3LYP/6-311++G (d,p) level, Table 5 displays the natural electronic configuration of compound 3, active sites, as well as the natural charge and population of total electrons on the subshells. Cl18 was more likely to accept electrons if it was more positively charged. N12, O15, and O17 atoms were the most negative center atoms, receiving electrons from molecule 3 static energy. Furthermore, in natural population analysis, there are 100 coordinated electrons in total Lewis and total non-Lewis structures for compound 3 (c.f. Table S2).

NonLinear Optical (NLO) analysis

The NonlLinear Optics (NLO) of the current compound has never been investigated before. The polarizabilities and hyperpolarizabilities of compound 3 were examined using B3LYP/6-311++G to investigate the relation between molecular structure and NLO (d,p). The approximate non-linear optical properties are shown in Table S3. One of the most important properties of the NLO system is the degree of molecular hyperpolarizability (β), which is 20 times more effective than P-nitroaniline (PNA) (standard prototype reference). As a result, the compound 3 structure appears to be a possible NLO material, and due to delocalization, the π-electrons have high electronic polarizability. Another crucial ability of semiconducting organic materials to transfer electric current and absorb photons in the ultraviolet-visible region of solar radiation is the very short diffusion period of exactions, which are important intercedes in the power change process [48-49].

Thermodynamic properties

Table S4 displays the calculated thermodynamic parameters (such as Zero-Point Vibrational Energy (ZPVE), thermal energy, specific heat capacity, rotational constants, and entropy S_{Vib} (T)), for compound **3** calculated using B3LYP/6-311++G (d,p) at 298K and 1.00 atm pressure. Compound **3** has a greater entropy value but a decrease in the value of the rotational constants. The ZPVEs (zero-point vibrational energy) appear to be highly variable. The thermal energies are similarly following the global minimum energy trend. Table 6 records the main statistical thermodynamic functions for compound **3**: heat capacity (C), entropy (S), and enthalpy changes (H) calculated from theoretical harmonic frequencies using vibrational analysis at the B3LYP/6-311++G(d,p) level. These thermodynamic functions increase with temperature varying from 200 to 600 K, as illustrated in Table 6 since molecular vibrational intensities increase with temperature [50]. Heat capacities, entropies, enthalpy changes, and temperatures were all fitted using quadratic formulas; the corresponding fitting factors (R2) for these thermodynamic characteristics are 0.99988, 0.99999, and 0.99988, respectively. Fig. S3 shows the relevant fitting equations and correlation graphs for those as follows:

Table S3: Total static dipole moment (μ), the mean polarizability (<α>), the anisotropy of the polarizability (Δα), and the mean first-order hyperpolarizability (<β>), for studied compound 3 by B3LYP/6-311++G (d,p)

Property	PNA	3
μ_x		-6.7839 Debye
μ_y		-1.7169 Debye
μ_z		0.1721 Debye
μ	2.44 Debye [a]	6.9999 Debye
α_{XX}		-124.2609 a.u.
α_{XY}		-9.6431 a.u.
α_{YY}		-75.6116 a.u.
α_{ZZ}		-92.5943 a.u.
α_{YZ}		-1.1935 a.u.
α_{XZ}		3.0791 a.u.
<α>	22×10^{-24} cm[3b]	35.25×10^{-24} esu
Δα		46.31×10^{-24} esu
βxxx		247.2045 a.u.
βxxy		31.7250 a.u.
βxyy		5.0827 a.u.
βyyy		54.4033 a.u.
βxxz		-23.0361 a.u.
βxyz		-1.5676 a.u.
βyyz		-3.6459 a.u.
βxzz		41.5856 a.u.
βyzz		1.5336 a.u.
βzzz		5.7093 a.u.
<β>	15.5×10^{-30} esu[c]	25.16×10^{-30} esu
DR		0.35
β_{HRS}		45.25

[a, b, c] PNA results are taken from references [29-30].

Table 6: Thermodynamic properties at different temperatures of 3 at the B3LYP/6-311++G(d,p)

T (K)	H^0_m *(kcal/mol)*	$C^0_{p,m}$ *(cal/mol K)*	S^0_m *(cal/mol K)*
200	116.14	50.80	120.10
250	118.93	60.74	132.96
300	122.20	69.93	145.23
350	125.91	78.31	156.95
400	130.01	85.87	168.18
450	134.48	92.64	178.92
500	139.27	98.66	189.21
550	144.33	104.00	199.06
600	149.66	108.75	208.49

Table S4: Calculated thermodynamically parameters for studied compound 3 at the B3LYP/6-311++G(d,p)

Parameters	**3**
Zero Point Vibrational Energy (kcal.mol^{-1})	84.40963
Rotational constant (GHz)	
A	1.43044
B	0.53017
C	0.38683
Entropy Total (S) (cal mol^{-1} K^{-1})	100.485
Translational	41.709
Rotational	31.372
Vibrational	27.405
Thermal Energy Total (E) (kcal mol^{-1})	90.952
Translational	0.889
Rotational	0.889
Vibrational	89.174
Specific heat (C_V) (cal mol^{-1} K^{-1})	40.672
Translational	2.981
Rotational	2.981
Vibrational	34.710

$C^0_{p,m,\,3} = 7.80349 + 0.12608\,T - 2.79319\times10^{-4}\,T2$; (R2 = 0.99998) , (2)

$S^0_{m,\,3} = 64.89967 + 0.15765\,T + 1.82708\times10^{-4}\,T2$; (R2=0.99999), (3)

$H^0_{m,\,3} = 85.61953 - 0.04695\,T + 2.29806\times10^{-4}\,T2$; (R2 = 0.99988), (4)

All the thermodynamic information is suitable for compound 3 research. They can be applied in the thermochemical field to compute other thermodynamic energies using thermodynamic function relationships and to estimate chemical reaction directions using the second law of thermodynamics. All thermodynamic calculations were done in the gas phase; hence they couldn't be used on a solution.

NMR analysis

Detailed data about NMR in 3-chloro-4-hydroxyquinolin-2(1H)-one (3) at B3LYP/6-311++G(d,p) in comparison between experimental NMR parameters are summarized in Table 7. The calculated ^{13}C and ^{1}H NMR

Table 7: ^{13}C and ^{1}H NMR chemical shifts (in ppm) calculated at the B3LYP/6-311++G(d,p) level of theory for of 3-chloro-4 hydroxyquinolin-2(1H)-one (3) using the GIAO method in DMSO

	3	Exp.
^{13}C chemical shifts		
C1	162. 75	167.00
C2	104.25	109.40
C3	130.51	134.70
C4	125.62	129.50
C5	132.04	136.50
C6	126.22	130.20
C7	128.53	133.70
C8	141.87	146.20
C9	150.37	156.00
^{1}H chemical shifts		
H10	7.83	7.70
H11	8.62	8.49
H13	7.88	7.63
H14	8.11	7.78
H16	7.96	7.73
H19	8.43	8.55
H-O/N	14.76	14.22

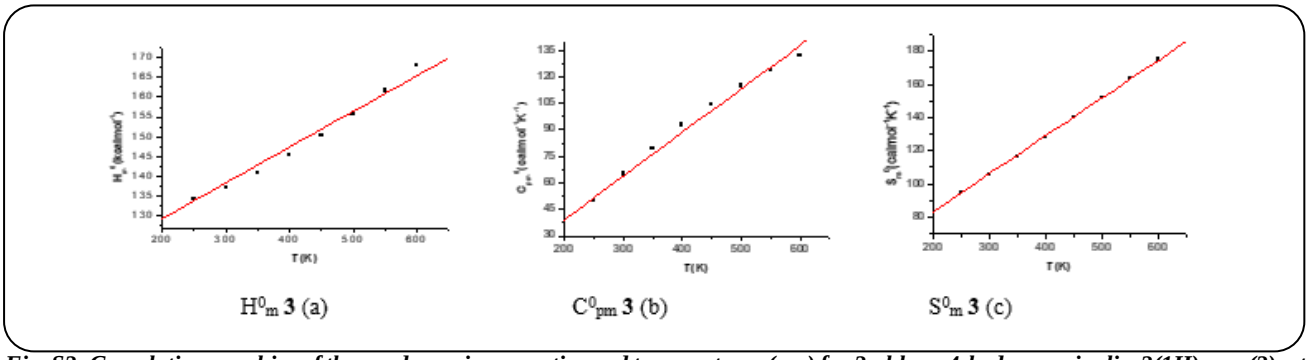

Fig. S3: Correlation graphics of thermodynamic properties and temperatures (a-c) for 3-chloro-4-hydroxyquinolin-2(1H)-one (3), at the B3LYP/6-311++G (d,p)

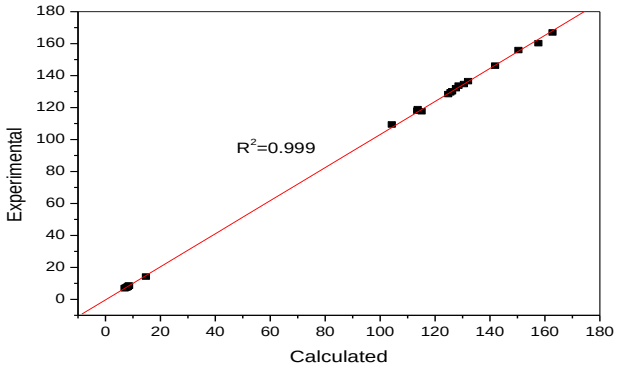

Fig. S4: Plot of the experimental chemical shifts verses the calculated ^{13}C and ^{1}H NMR chemical shifts at the B3LYP/6-311++G(d,p) level of theory 3-chloro-4 hydroxyquinolin-2(1H)-one (3) using the GIAO method in DMSO

chemical shifts for 3-chloro-4 hydroxyquinolin-2(1H)-one (3) in DMSO show good agreement with the experimental findings. Plotting of calculated ^{13}C and ^{1}H NMR chemical shifts against experimental values of 3-chloro-4 hydroxyquinolin-2(1H)-one (3) is displayed in Fig. S4. A high correlation between calculated and experimental results of 3-chloro-4 hydroxyquinolin-2(1H)-one (3) was noticed which gives confidence on the used computational procedures. From Table 7, C_2 in the 3-chloro-4 hydroxyquinolin-2(1H)-one (3) has the highest chemical shift (161.82/162.75 ppm) that can be attributed to its closeness to the oxygen atom. H_{11} of the 3-chloro-4 hydroxyquinolin-2(1H)-one (3) has the highest chemical shift (8.62/8.65 ppm). Therefore, the calculated ^{1}H NMR chemical shifts help in predicting the presence or absence of HB.

Table 8: In vitro antimicrobial activities of the synthesized compounds at 500 and 1000 µg/mL and the MIC values for some selected compound 3

Compd.	Conc. (µg/ml)	Zone of inhibition in mm* and (MIC values in µg/mL)					
		Bacteria Gram (+) ve		Bacteria Gram (−) ve		Yeast	Fungi
		S. aureus	*B. subtilis*	*S. typhimurium*	*E. coli*	*C. albicans*	*A. fumigatus*
3	500	-	-	-	-	14 (250)	-
	1000	-	-	-	-	20	-
S**	500	26	25	28	27	28	26
	1000	35	35	36	38	35	37

* Low active: 6–12 mm; moderately active: 13–19 mm; highly active: 20–30 mm; –: No inhibition or inhibition less than 5 mm.
S**: Standard drugs

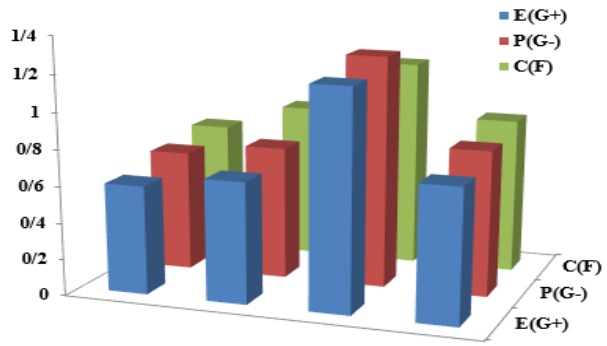

Fig. S5. Antimicrobial activity for 3-chloro-4-hydroxyquinolin-2(1H)-one (3), against gram-positive bacteria (G^+), gram-negative bacteria (G^-), and Fungi (F)

Antimicrobial activity

The antibacterial and antifungal properties of produced compound 3 were tested against Gram-positive *S. aureus* and *B. subtilis*, and Gram-negative *S. Typhimurium* and *E. Coli*, as well as *yeast*, *C. albicans*. *A. fumigatus* is a species of *A. fumigatus*. Table 8 and Fig. S5 show the findings of measuring the growth inhibition (zone of inhibition) around the disc of material. Antibiotics were evaluated for antibacterial activity and found to be ineffective against all bacteria and fungi. The small size of compound 3 enhances its absorption ability on the surface of the cell wall of microorganisms and the cell respiration process, which explains why it has such significant antibacterial action against all bacteria and fungi tested in compound 3. As a result, compound 3 is required for the growth-inhibitor effect to occur.

Structure-Activity Relationship (SAR)

The biological activity of synthesized molecule **3** can be related to the expected ground state energetic and global properties. According to (Tables 2 and 8) compound **3** has biological activity experimentally against G+, G-, and fungi. The energy gap, Eg, of the studied compound computed at B3LYP/6-311++G (d,p) follows the same experimentally determined sequence, telling that Eg is one factor contributing to the reactivity of the studied compound, along with E_{HOMO}, which measures the donating power, and dipole moment which measures the charge separation. The calculated theoretically global softness (S), global electrophilicity index (ω), electronegativity (χ), and chemical potential (V) of the studied compound **3** follow the same practical biological activity. The chemical hardness (η) in reverse follows the experimental biological activity. Natural charge from NBO and mean first-order hyperpolarizability (β) have incompatible with the experimental biological activity.

Acidity and basicity

Our investigated compound has two labile protons which are attached to either nitrogen or oxygen atoms. The reliable and quick estimation of the acidity and basicity of a molecule without synthesis and experimental determination is very important to interpret the structure reactivity and property relationships. Moreover, knowledge of the acidity constants, (pKa) is important for determining the equilibrium constant (K) of reactions, especially that involving proton transfers. However, when the determination of pKa experimentally is difficult, computational approaches can be applied to estimate the pKa using the thermodynamic free energies cycle that is shown in Scheme 2. Consequently, DFT calculations were applied to study the protonated (cation) and deprotonated (anion) forms of the 3-chloro-4-hydroxyquinolin-2(1H)-one (3) that are depicted in Fig. 4. The protonated form,

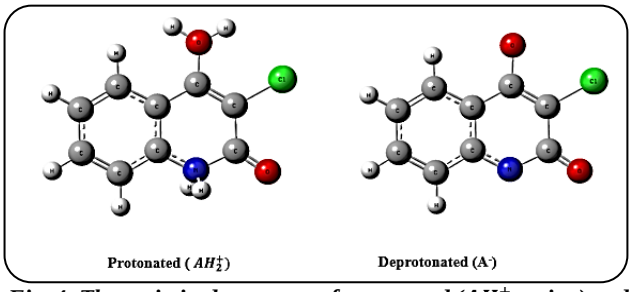

Fig. 4: The optimized structure of protonated (AH_2^+,cation) and deprotonated (A^-, anion) forms of 3-chloro-4-hydroxyquinolin-2(1H)-one (3) at B3LYP/6-311++G(d,p)

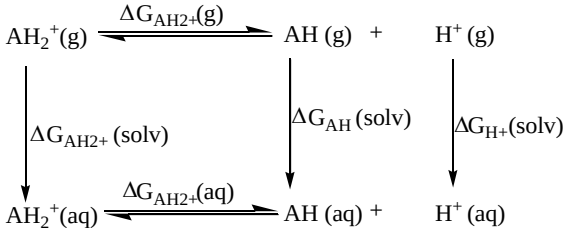

Scheme 2: Thermodynamic cycle connecting gas (g) and aqueous (s) phase for pKa calculation

denoted AH_2^+, typically has a net charge of +1, while the corresponding 3-chloro-4-hydroxyquinolin-2(1H)-one (3), AH, is typically neutral. Therefore, throughout the acidity constant calculation from the protonated form we will consider the energy of the 3-chloro-4-hydroxyquinolin-2(1H)-one (3). The deprotonated form denoted A^-, typically has a net charge of -1. The equations used for calculating pKa values are given below:

$$pK_a = \Delta G_{AH_2^+}(aq) \,/\, 2.303RT \quad (5)$$

$$\Delta G_{AH_2^+}(aq) = \Delta G_{AH_2^+}(g) + \Delta\Delta G_{AH_2^+}(solv) \quad (6)$$

$$\Delta G_{AH_2^+}(g) = G_{AH}(g) + G_{H^+}(g) - G_{AH_2^+}(g) \quad (7)$$

$$\Delta\Delta G_{AH_2^+}(\text{solv}) = \Delta G_{AH}(\text{solv}) + \Delta G_{H^+}(\text{solv}) - \Delta G_{AH_2^+}(\text{solv}) \quad (8)$$

where $G_i(g)$ is the standard free energy of the species "i" in the gas phase, $\Delta G_i(solv)$ is the solvation free energy of "i" and $G_i(aq)$ is the free energy change in the aqueous phase. The $G_{H^+}(g)$ and $\Delta G_{H^+}(solv)$ terms are –6.28 kcal/mol [51,52] and –265.90 kcal/mol [53,54] respectively.

The experimental acidity constants were taken in our consideration. The correlation between the experimental and the calculated acidity constants revealed that the B3LYP/6-311++G(d,p) level yields the closest pKa value to the experimental values.

The experimental pKa of 3-chloro-4-hydroxyquinolin-2(1H)-one (3) was reported as 12.7 [55] and the calculated pKa from the protonation form is found as 15.54, using B3LYP/6-311++G(d,p), level. By comparing the pKa obtained by deprotonation, we can find that the 3-chloro-4-hydroxyquinolin-2(1H)-one (3) is a weaker acid. This can be attributed to the strength of the OH and NH bonds, the presence or absence of hydrogen bonds, and the stability of the resulting conjugate base upon deprotonation.

Electronic absorption spectra

The main contributions to the UV-visible spectra of the title compound 3 were discovered and summarized in Table S5 using theoretical calculations. Fig. 5 describes the experimental UV-Visible and theoretical spectra. As indicated in Table S5, the absorption wavelengths in gas phase transitions were 288, 221, 211, 205, and 195 nm, with energy gaps of 4.30, 5.61, 5.88, 6.05, 6.37 eV and oscillator strengths of 0.2073, 0.1152, 0.4807, 0.1318, 0.2992, respectively. Based on oscillator strength and absorption coefficient values, only the first transition will have substantial absorption intensity, implying that the band at wavelength 288 nm will have the highest intensity, with a HOMO-LUMO contribution of 94%. The absorption wavelengths for the ethanol phase, which was also measured at 286, 256, 214, 210, and 197 nm, with energy gaps of 4.34, 4.84, 5.79, 5.84, 6.28 eV and oscillator strengths of 0.2316, 0.1669, 0.8933, 0.1436, 0.2994, respectively, with a HOMO-LUMO contribution of 97%. In this condition, the HOMO-LUMO contribution is strongest in the early transition.

The initial singlet excited state's absorption wavelength in the gas phase is 288 nm, with an oscillator strength of 0.2073. The identical absorption bands are found at 286 and 289 nm in ethanol and dioxane solvents, with oscillator strengths of 0.2316 and 0.2879, respectively. An increase in polarity causes a rise in absorption wavelength, resulting in a red shift. This means that the excited state becomes more stable as the polarity of the excited state increases. The UV-Vis absorption bands for the initial singlet excited state S0—>S1 in ethanol and dioxane are observed at 360 nm and 380 nm, respectively. This implies that theoretical and experimental UV-Vis results are linked.

Table S5: Experimental and Computed excitation energies (in eV), electronic transition configurations, and oscillator strengths [a] (f) for the optical transitions of the absorption bands in the UV-Vis. regions (involving HOMOs) of the compound 3 at the CAM-B3LYP/6-311++G (d,p)

Medium	Transition	Excitation energies	Type of transition	$\lambda_{max/\mathrm{nm}}$ *Th and Ex.*	Oscillator strengths (f)	Configuration composition corresponding transition orbital
Gas phase	S0—>S1	4.30	n-π*	288	0.2073	-0.21(49 ->51); -0.16(49 ->53); 0.64(50 ->51)
	S0—>S2	5.61	π-π*	221	0.1152	-0.26(49 ->51); 0.40(50 ->52); 0.43(50 ->53); 0.12(50 ->55); -0.12(50 ->56)
	S0—>S3	5.88	π-π*	211	0.4807	-0.20(47 ->51); 0.21(49 ->52); 0.54(49 ->53); 0.17(50 ->51); 0.16(50 ->54); 0.11(50 ->56)
	S0—>S4	6.05	π-π*	205	0.1318	0.19(47 ->51); 0.16(47 ->53); 0.13(49 ->53); 0.20(50 ->53); 0.58(50->56)
	S0—>S5	6.37	π-π*	195	0.2992	0.61(47 ->51); -0.23(49 ->53); -0.17(50 ->56)
Ethanol	S0—>S1	4.34	n-π*	286 360	0.2316	-0.16(49 ->51); 0.11(49 ->52); -0.13(49 ->53); 0.65 (50 ->51)
	S0—>S2	4.84	n-π*	256 310	0.1669	0.63(49 ->51); 0.15(50 ->51); -0.16(50 ->52); 0.19(50 ->53)
	S0—>S3	5.79	π-π*	214 235	0.8933	0.16(49 ->51); -0.25(49 ->52); 0.31(49 ->53); 0.14(50 ->51); 0.36(50 ->52); -0.13(50 ->53)
	S0—>S4	5.84	π-π*	210	0.1436	0.10(45 ->51); 0.17(49 ->52); 0.31(49 ->53); -0.23(50 ->52); 0.38(50 ->55); -0.13(50 ->56)
	S0—>S5	6.28	π-π*	197	0.2994	0.46(47 ->51); -0.22(48 ->51); 0.15(49 ->52) -0.22(49 ->53); -0.36(50 ->56)
Dioxane	S0—>S1	4.28	n-π*	289 380	0.2879	-0.18(49 ->51); -0.14(49 ->53); 0.65 (50 ->51)
	S0—>S2	4.81	n-π*	257 315	0.1482	0.61(49 ->51); 0.18(50 ->51); 0.26(50 ->53)
	S0—>S3	5.68	π-π*	218 255	0.5196	-0.27(49 ->51); -0.12(49 ->53); 0.20(50 ->52); 0.58(50 ->53)
	S0—>S4	5.80	π-π*	214	0.1959	0.38(49 ->53); -0.11(49 ->54); -0.35(50 ->52); 0.18(50 ->53); -0.19(50 ->55); 0.21(50 ->56)
	S0—>S5	6.26	π-π*	198	0.2644	0.59(47 ->51); -0.20(49 ->53); 0.11(49 ->56); 0.26(50 ->56)

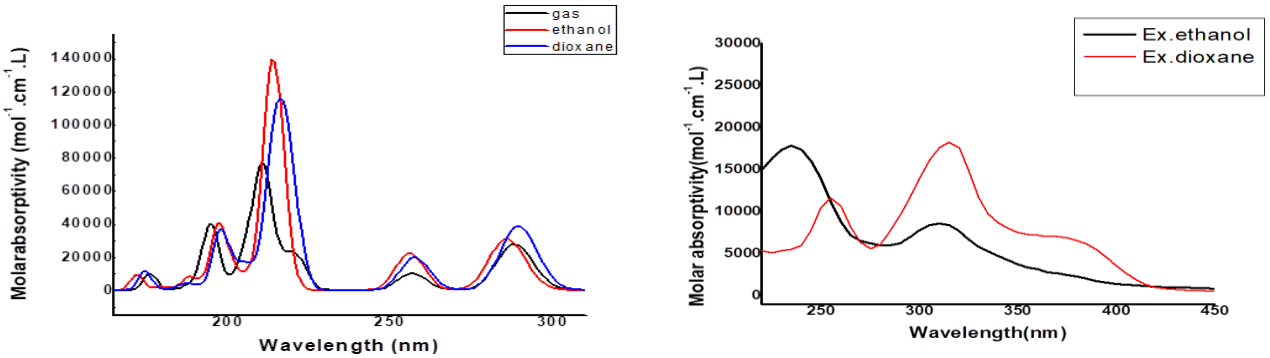

Fig. 5: Electronic absorption spectra of 3-chloro-4-hydroxyquinolin-2(1H)-one (3), (a) experimental in ethanol, (b) experimental in dioxane (c) theoretical in gas phase (d) theoretical in ethanol, (e) theoretical in dioxane

Furthermore, the other singlet excited states were investigated in the same attitude. The effect of increasing polarity was discovered to cause a blue shift in absorption wavelengths. n-π* transitions cause (H→L) transition that occurs in both phases. In the gas phase, the second singlet excited state S0—>S2 was detected at 221 nm, whereas in ethanol and dioxane, it was observed at 256 and 257 nm, respectively. This value matched the experimental values found

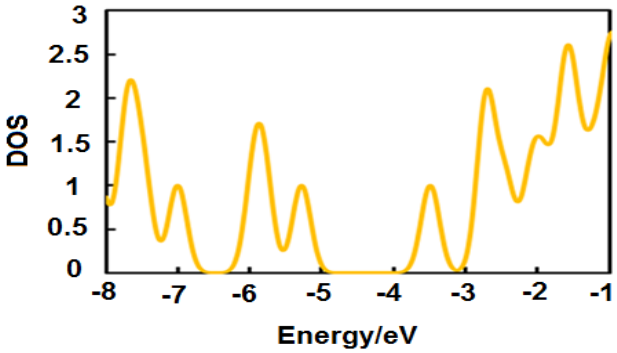

Fig: S6 Density of states (DOSs) spectrum of compound 3

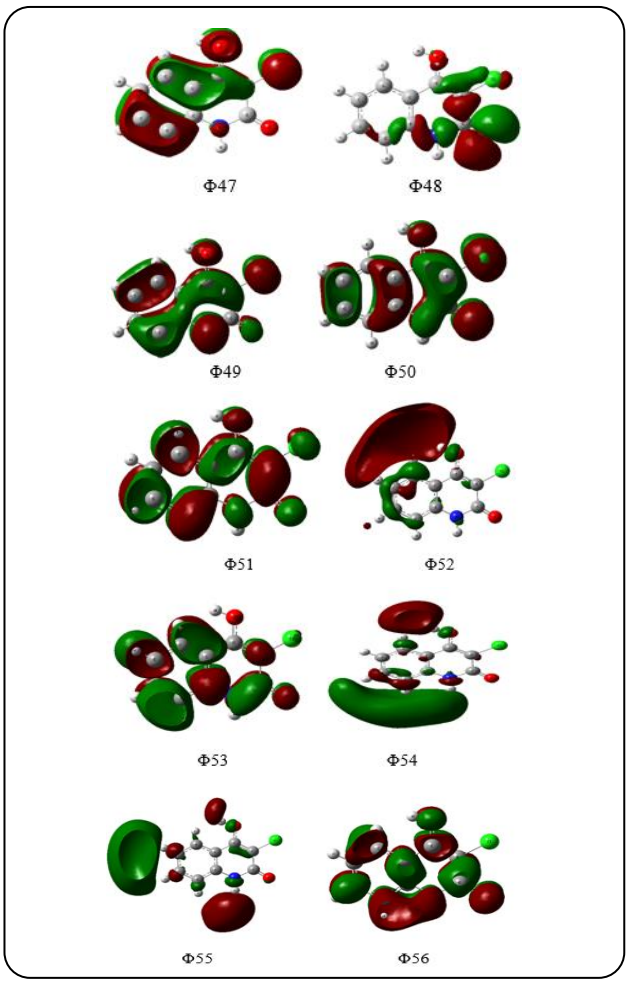

Fig. S7: Electron density contours of 3-chloro-4-hydroxyquinolin-2(1H)-one (3)

at 310 and 315 nm in ethanol and dioxane, respectively. As the polarity of the solvent changes from dioxane to ethanol, the spectrum bands for the excited and ground states have the same values; additionally, the strength of the bands rises with polar solvents, resulting in all bands changing to (π-π*).

The UV/vis spectra of the title compound 3 in the gas phase and two solvents in all singlets excited states S0—>S5 are shown in Table S5. Finally, there is good agreement between theoretical and experimental UV-Visible observations. As illustrated in Fig. S6, the GaussSum3 program [56] was used to plot a visual description of the DOS of molecule 3. The nature of the electronic transition was used to deduce the electron density contours of molecular orbitals. The assigned of these bands shows localized, delocalized and Charge Transfer CT character (Fig. S7).

CONCLUSIONS

Chlorination of 3-acetyl-4-methylthioquinolin-2(1H)-one (1) with sulfuryl chloride may lead to 3-(2,2-dichloroacetyl)-4-methylthioquinolin-2(1H)-one (2). Whereas analytical and spectral results for the product of this reaction evoked the proposal of obtaining 3-chloro-4-hydroxyquinolin-2(1H)-one (3), which was found by reduction of 3,3-dichloroquinolin-2,4-dione. Electronic dispersion and NBO analysis were used to validate the stability of the title compound 3. Experimental and theoretical vibrational wavenumbers were found to be in good agreement. The molecule is soft (low energy gap), electrophilic (high electrophilicity index), and reactive (low hardness), according to HOMO, LUMO, and global reactivity descriptors. The quinoline ring's skeleton and the molecule's edges exhibited zero potential, according to MEP analysis. To understand the electronic transitions of the title compound 3, TD-DFT calculations were performed on the electronic absorption spectra in the gas phase and solvent. In comparison to the PNA molecule, the created molecule offers good benefits in technology-related applications, according to the NLO study. The chemical's thermodynamic properties were also calculated. Temperature-statistical thermodynamics relationships were also discovered.

Received : Dec.01, 2022 ; Accepted : Apr.03, 2023

REFERENCES

[1] Sarveswari S., Vijayakumar V., Siva R., Priya R., Synthesis of 4-Hydroxy-2(1H)-Quinolone Derived Chalcones, Pyrazolines and Their Antimicrobial, in Silico Antimalarial Evaluations, *Appl. Biochem. Biotechnol.*, **175**: 43-64 (2015).

[2] Narwal S., Kumar S., Verma P.K., Synthesis and Therapeutic Potential of Quino-Line Derivatives, *Res. Chem. Interned.*, **43**: 2765–2798 (2017).

[3] Martinez P., Krake S., Poggi M., Campbell S., Willis P., Dias L., 2,3,8-Trisubsti-Tuted Quinolines with Antimalarial Activity, *An. Acad. Bras. Cienc.*, **90**: 1215–1231 (2018).

[4] Casal J., Asís S., Natural and Synthetic Quinoline Derivatives as Antituberculosis Agents, *Tuberc. Res. Treat.*, **2**: 1007 (2017).

[5] Shang X.F., Morris-Natschke S.L., Liu Y.Q., Guo X., Xu X.S., Goto M., Li J.C., Yang G.Z., Lee K.H., Biologically Active Quinoline and Quinazoline Alkaloid's part I, *Med. Res. Rev.*, 38: 775–828 (2018).

[6] Mopuri D., Syed S.V., Madhulatha A., Docking, Synthesis and Biological Evaluation of Novel Quinoline Containing Schiff Bases for Anti-Inflammatory and Antioxidant Activities, *Int. J. Pharm. Sci. Res.*, **11**: 721–731 (2020).

[7] Li K., Li Y., Zhou D., Fan Y., Guo H., Ma T., Wen J., Liu D., Zhao L., Synthesis, and Biological Evaluation of Quinoline Derivatives as Potential Anti-Prostate Cancer Agents and Pim-1 Kinase Inhibitors, *Bioorg. Med. Chem.*, **24**: 1889–1897 (2016).

[8] Ahsan M.J., Shastri S., YYadav R., Hassan M.Z., Bakht M.A., Jadav S.S., Yasmin S., Synthesis and Antiproliferative Activity of Some Quinoline and Oxadiazole Derivatives, *Org. Chem. Int.*, **2016**: 1–10 (2016).

[8] Chabukswar A.R., Kuchekar B.S., Jagdale S.C., Lokhande P.D., Chabuk-swar V.V., Shisodia S.U., Mahabal R.H., Londhe A.M., Ojha N.S., Synthesis and Evaluation of Analgesic, Anti-Asthmatic Activity of (E)-1-(8-Hydroxyquinolin-7-yl)-3-Phenylprop-2-en-1 Ones, *Arab. J. Chem.*, **9**: 704 –712 (2016).

[9] Zielger E., Salvador R., Kapp Th., Synthesen Von Heterocyclen, 41, Mitt: -Uber Cyclische Dichlormalonyl-Verbindungen, *Monatsh Chem.*, **93**: 1376-1382 (1962).

[10] Abdel Halim S., Ibrahim M.A., Synthesis, DFT computational insights on Structural, Optical, Photoelectrical Characterizations and Spectroscopic Parameters of the Novel (2E)-3-(4-Methoxy-5-oxo-5H-furo[3,2-g] Chromen-6-yl) Acrylonitrile (MOFCA), *J. Mol. Struct.*, **1223**: 129316-129331 (2021).

[11] Abdel-Halim S., Ibrahim M.A., Synthesis, Synthesis, FT-IR, Structural, Thermochemical, Electronic Absorption Spectral, and NLO Analysis of the Novel 10-Methoxy-10H-furo[3,2-g] Chromeno[2,3-b] [1,3] Thiazolo[5,4-e] Pyridine-2,10(3H)-Dione (MFCTP): a DFT/TD-DFT Study, *RSC Adv.*, **11**: 32047–32066 (2021).

[12] Abdel Halim S., Ibrahim M.A., Synthesis, Density Functional Theory Band Structure Calculations, Optical, and Photoelectrical Characterizations of the Novel (9-Bromo-3-Cyano-5-Oxo-1,5-Dihydro-2H-Chromeno[4,3-b] Pyridin- 2ylidene) Propanedinitrile, *J. Heterocyclic Chem.*, **56**: 2542-2554 (2019).

[13] Abdel Halim S., Ali L.I., Sanad S.G., Theoretical Calculations of Solvation 12-Crown-4 ($12CN_4$) in Aqueous Solution and its Experimental Interaction with Nano $CuSO_4$, *Int. J. Nano Dimens.*, **8**: 142-158 (2017).

[14] Abdel Halim S., Khalil A.K., TD-DFT calculations, NBO Analysis and Electronic Absorption Spectra of Some Thiazolo[3,2-a] Pyridine Derivatives, *J. Mol. Struct.*, **1147**: 651-667 (2017).

[15] Abdel Halim S., Ibrahim M.A., Synthesis, DFT Calculations, Electronic Structure, Electronic Absorption Spectra, Natural Bond Orbital (NBO) and Nonlinear Optical (NLO) Analysis of the Novel 5-Methyl-8H-benzo[h]Chromeno[2,3-b] [1,6] Naphthyridine-6(5H),8-Dione (MBCND), *J. Mol. Struct.*, **1130**: 543–558 (2017).

[16] Govindarajan M., Karabacak M., FT-IR, FT-Raman, and UV Spectral Investigation; Computed Frequency Estimation Analysis and Electronic Structure Calculations on 4-Hydroxypteridine, *J. Mol. Struct.*, **1038**: 114–125 (2013).

[17] Asif Mahmood, Salah Ud-Din Khan, Usman Ali Rana, Mudassir Hussain Tahir, Red Shifting of Absorption Maxima of Phenothiazine Based Dyes by Incorporating Electron-Deficient Thiadiazole Derivatives as P-Spacer, *Arabian Journal of Chemistry*, **12**: 1447–1453 (2019).

[18] Asif Mahmood, Salah Ud-Din Khan, Fazal ur Rehman, Assessing the Quantum Mechanical Level of Theory for Prediction of UV/Visible Absorption Spectra of Some Aminoazobenzene Dyes, *Journal of Saudi Chemical Society*, **19**: 436–441 (2015).

[19] Asif M., Muhammad S., Muhammad A., Muhamma d Imran A., Bilal K., Theoretical Investigation for the Designing of Novel Antioxidants, *Canadian Journal of Chemistry*, **91**: 0356 (2012).

[20] Ahmed S., Zainab Al S., Synthesis, Characterization and Antimicrobial Activity of Some New Tetrazole Derivatives from Hydrazones, *Iran. J. Chem. Chem. Eng. (IJCCE)*, **41(7)**: 2247-2262, (2022).

[21] Gaussian 09, Revision A.1, Frisch M.J., Trucks G.W., Schlegel H.B., Scuseria G.E., Robb M.A., J. Cheeseman R., Scalmani G., Barone V., Mennucci B., Petersson G.A., H Nakatsuji., Caricato M., Li X., Hratchian H.P., Izmaylov A.F., Bloino J., Zheng G., Sonnenberg J.L., Hada M., Ehara M., Toyota K., Fukuda R., Hasegawa J., Ishida M., Nakajima T., Y Honda., Kitao O., Nakai H., Vreven T., Montgomery J.A., Jr., Peralta J.E., F Ogliaro., M Bearpark., Heyd J.J., Brothers E., Kudin K.N., Staroverov V.N., Kobayashi R., Normand J., Raghavachari K., Rendell A., Burant J.C., Iyengar S.S., J Tomasi., Cossi M., Rega N., Millam J.M., Klene M., Knox J.E., J. Cross B., Bakken V., Adamo C., Jaramillo J., Gomperts R., Stratmann R.E., Yazyev O., Austin A.J., Cammi R., Pomelli C., Ochterski J.W., R Martin.L., Morokuma K., Zakrzewski V.G., Voth G.A., Salvador P., Dannenberg J.J., Dapprich S., Daniels A.D., Farkas O., Foresman J.B., Ortiz J.V., Cioslowski J., Fox D.J., Gaussian, Inc., Wallingford CT, (2009).

[22] GaussView, Version 5, Dennington R., Keith T., Millam J., Semichem Inc., Shawnee Mission KS, (2009).

[23] Shahab S., Kumar R., Darroudi M., Borzehandani M.Y., Molecular Structure and Spectroscopic Investigation of Sodium (E)-2-Hydroxy-5-((4-Sulfonatophenyl) Diazenyl) Benzoate: A DFT Study, *J. Mol. Struct.*, **1083**: 198–203 (2015).

[24] Irfan A., Al-Sehemi A.G., Kalam A., Structural, Electronic and Charge Transfer Studies of Dianthra[2,3-b:2′,3′-f]Thieno[3,2-b]Thiophene and its Analogues: Quantum Chemical Investigations, *J. Mol. Struct.*, **1049**: 198–204 (2013).

[25] Irfan A., Al-Sehemi A., Muhammad S., Investigating the Effect of Acene-Fusion and Trifluoroacetyl Substitution on the Electronic and Charge Transport Properties by Density Functional Theory, *Synth. Met.*, **190**: 27–33 (2014).

[26] Becke A.D., Density-Functional Thermochemistry. III. The Role of Exact Exchange, *J. Chem. Phys.* **98**: 5648–5652 (1993).

[27] Yanai T., Tew D., Handy N., A New Hybrid Exchange–Correlation Functional Using the Coulomb-Attenuating Method (CAM-B3LYP) *Chem. Phys. Lett.*, **393**: 51–57 (2004).

[28] Lee C.T., Yang W.T., Parr R.G.B., Development of the Colle-Salvetti Correlation-Energy Formula into a Functional of the Electron Density, *Phys. Rev.*, **37**: 785–790 (1988).

[29] Petersson D.A., Allaham M.A., A Complete Basis Set Model Chemistry. II. Open-Shell Systems and the Total Energies of the First-Row Atoms, *J. Chem. Phys.* **94**: 6081–6090 (1991).

[30] Wolinski K., Hinton J.F., Pulay P., Efficient Implementation of the Gauge-Independent Atomic Orbital Method for NMR Chemical Shift Calculations, *J. Am. Chem. Soc.*, **112**: 8251–8260 (1990).

[31] Sarafran M., Komasa A., Adamska E.B., Molecular Structure, Vibrational Spectroscopic (FT-IR, FT-Raman), UV and NBO Analysis of 2-Chlorobenzonitrile by Density Functional Method, *J. Mol. Struct.*, **827**: 101–107 (2007).

[32] Khoshtarkib Z., Ebadi A., Alizadeh R., Ahmadi R., Amani V., Dichloridobis (Phenanthridine- κN) Zinc (II), *Acta Crystallographica Section E: Structure Reports Online*, **65**: (2009).

[33] Amani V., Ahmadi R., Naseh M., Ebadi A., Synthesis, Spectroscopic Characterization, Crystal Structure and Thermal Analyses of Two Zinc (II) Complexes with Methanolysis of 2-Pyridinecarbonitrile as a Chelating Ligand, *Journal of the Iranian Chemical Society* **14**: 635–642 (2017).

[34] Afshar, M. Adsorption of Lomustin Anticancer Drug on the Surface of Carbon Nanotube: A Theoretical Study. *Eurasian Chemical Communications*, **2**: 595–603 (2020).

[35] Shahzad H., Ahmadi R., Adhami F., Najafpour J., Adsorption of Cytarabine on the Surface of Fullerene C20: A Comprehensive DFT Study, *Eurasian Chemical Communications*, **2**: 162–169 (2020).

[36] Young D.C., "Computational Chemistry: A Practical Guide for Applying Techniques to Real World Problems (Electronic)", John Wiley & Sons Inc., New York, (2001).

[37] Lambert J.B., Shurvell H.F., Vereit L., Cooks R.G., Stout G.H., "Organic Structural Analysis", Academic Press, New York, (1976).

[38] Kalsi P.S., Spectroscopy of Organic Compounds, *Academic Press*, New York, (2002).

[39] Macoonald J.N., Mackay S.A., Tyler J.K., Cox A.P., Ewart I.C. Science of Synthesis: Houben-Weyl Methods of Molecular Transformations, *J. Chem. Soc. Faraday Trans.* II., **77**: 79-89 (1981).

[40] Sajan D.Y., Erdogdu R.O., Reshmy K., Dereli K., Thomas K., Hubert I., DFT-Based Molecular Modeling, NBO Analysis and Vibrational Spectroscopic Study of 3- (Bromoacetyl) Coumarin, *J. Spectrochim. Acta A*, **82**: 118 – 125 (2011).

[41] Lide D. R., The Chemistry of Organic Sulfur Compounds, *Tetrahedron.* **17**: 125-135 (1962).

[42] Duan X., Huang Y., Cui Y., Wang J., Lieber C.M., Indium Phosphide Nanowires as Building Blocks for Nanoscale Electronic and Optoelectronic Devices, *Nature* 66-69 (2001)

[43] Luque F.J., López J.M., Orozco M., Electrostatic Interactions of a Solute with a Continuum. a Direct Utilization of Ab Initio Molecular Potentials for the Prevision of Solvent Effects, *Theor. Chem. Acc.*, **103**: 343-345 (2000).

[44] Okulik N., Jubert A.H., Theoretical Analysis of the Reactive Sites of Non-Steroidal Anti-Inflammatory Drugs, *Int. Elect. J. Mol. Des.*, **4**: 17-30 (2005).

[45] Politzer P., Murray J.S., The Fundamental Nature and Role of the Electrostatic Potential in Atoms and Molecules, *Theor. Chem. Acc.*, **108**: 134-142 (2002).

[46] Nagabalasubramanian P.B., Periandy S., Mehmet K., Govindarajan M., Molecular Structure, Vibrational, Electronic, and thermal Properties of 4-Vinylcyclohexene by Quantum Chemical Calculations, *Spectrochim. Acta Mol. Biomol. Spectrosc.*, **145**: 340–352 (2015).

[47] Mariappan G., Sundaraganesan N., FT-IR, FT-Raman, NMR Spectra, Density Functional Computations of the Vibrational Assignments (for Monomer and Dimer) and Molecular Geometry of Anticancer Drug 7-Amino-2-Methylchromone, *J. Mol. Struct.*, **1063**: 192–202 (2014).

[48] Zhang C.R., Chen H.S., Wang G.H., Structure and Properties of Semiconductor Micro Clusters Gan Pn (N=1-4): *A First Principal Study. Res. Chin. U*, **20**: 640-646 (2004).

[49] Sun Y., Chen X., Sun L., Guo X., Lu W., Nanoring Structure and Optical Properties of Ga 8 As 8. *Chem. Phys. Lett.*, **381**: 397-403 (2003).

[50] Natorajan S., Shanmugam G., MartinCryst S.A., Technal Res., 43: 561-570 (2008) Chemia D.S., Zysss J., Orlando, FL, (1987) Bradshow D.S., Andrews D.L., *J. Nonlinear Opt. Phys. Matter*, **18**: 285-295 (2009).

[51] Topol I.A., Tawa G.J., Burt S.K., Rashin A.A., On the Structure and Thermodynamics of Solvated Monoatomic Ions Using a Hybrid Solvation *Model. J. Chem. Phys.*, **111(24)**: 10998–11014 (1999).

[52] Jang Y. H., Sowers L.C., Çağin T., Goddard W.A., First Principles Calculation of PKa Values for 5-Substituted Uracils, *J. Phys. Chem. A* 2001, **105**: 274–280 (2001).

[53] Tissandier M.D., Cowen K.A., Feng W.Y., Gundlach E., Cohen M.H., Earhart A.D., Coe J.V., Tuttle T.R., The Proton's Absolute Aqueous Enthalpy and Gibbs Free Energy of Solvation from Cluster-Ion Solvation Data,*J. Phys. Chem. A*, **102(40)**: 7787–7794 (1998).

[54] Camaioni D.M., Schwerdtfeger C.A., Comment on "Accurate Experimental Values for the Free Energies of Hydration of H^+ , OH^- , and H_3O^+." *J. Phys. Chem. A*, **109**: 10795–10797 (2005).

[55] Oda M., Sugiyama A., Takeuchi R., Fujiwara Y., Miyatake R., Abe T., Kuroda, S., Synthesis , Molecular Structure , and Properties of 2-(2-Hydroxyphenyl)-1- Azaazulene, *Eur. J. Org. Chem.*, **6**: 2231–2236 (2012).

[56] Rastogi V.K., Palafox M.A., Tanwar P.P., Mittal L., 3, 5-Difluorobenzonitrile: Ab initio Calculations, FTIR and Raman Spectra, *Spectrochim. Acta Part A: Mol. Biomol. Spectrosc.*, **58**: 1987-2004 (2002).